International Journal of Pharmaceutics 620 (2022) 121742

Contents lists available at ScienceDirect

International Journal of Pharmaceutics

journal homepage: www.elsevier.com/locate/ijpharm

Mathematical modelling of endovascular drug delivery: Balloons versus stents

Javier Escuer [a], André Fensterseifer Schmidt [b], Estefanía Peña [a,c], Miguel A. Martínez [a,c], Sean McGinty [b,d,*]

[a] Aragón Institute for Engineering Research (I3A), University of Zaragoza, Spain
[b] Division of Biomedical Engineering, University of Glasgow, Glasgow, UK
[c] Biomedical Research Networking Center in Bioengineering, Biomaterials and Nanomedicine (CIBER-BBN), Spain
[d] Glasgow Computational Engineering Centre, Division of Infrastructure and Environment, University of Glasgow, Glasgow, UK

ARTICLE INFO

Keywords:
Pharmacokinetics
Drug-coated balloons
Drug-eluting stents
Computational modelling

ABSTRACT

The most common treatment for obstructive coronary artery disease (CAD) is the implantation of a permanent drug-eluting stent (DES). Not only has this permanency been associated with delayed healing of the artery, but it also poses challenges when treating subsequent re-narrowing due to in-stent restenosis (ISR). Drug-coated balloons (DCBs) provide a potential solution to each of these issues. While their use has been primarily limited to treating ISR, in recent years, DCBs have emerged as an attractive potential alternative to DESs for the treatment of certain de novo lesions. However, there remain a number of concerns related to the safety and efficacy of these devices. Firstly, unlike DESs, DCBs necessitate a very short drug delivery window, favouring a higher drug loading. Secondly, while the majority of coronary DCBs in Europe are coated with paclitaxel, the potential mortality signal raised with paclitaxel DCBs in peripheral interventions has shifted efforts towards the development of limus-eluting balloons. The purpose of this paper is to provide a computational model that allows drug delivery from DCBs and DESs to be investigated and compared. We present a comprehensive computational framework that employs a 2D-axisymmetric geometry, incorporates two nonlinear phases of drug binding (specific and non-specific) and includes the influence of diffusion and advection, within a multilayer arterial wall. We utilise this framework to (i) simulate drug delivery from different types of balloon platform; (ii) explore the influence of DCB application time; (iii) elucidate the importance on release kinetics of elevated pressure during DCB application; (iv) compare DCB delivery of two different drugs (sirolimus and paclitaxel) and; (v) compare simulations of DESs versus DCBs. Key measures of comparison are related to safety (drug content in tissue, *DC*) and efficacy (specific binding site saturation, %*SBSS*) markers. Our results highlight the pros and cons of each device in terms of *DC* and %*SBSS* levels achieved and, moreover, indicate the potential for designing a DCB that gives rise to sufficiently similar safety and efficacy indicators as current commercial DESs.

1. Introduction

Coronary artery disease (CAD) is the leading cause of death globally (Roth et al., 2018). The most common treatment for obstructive CAD is percutaneous coronary intervention (PCI) where a stent is deployed to widen the artery and restore blood flow. Nowadays, the vast majority of stents deliver drug to the arterial wall (so-called drug-eluting stents [DESs]) to counteract the inflammatory response following deployment, with the aim of preventing excessive neointimal regrowth, known as restenosis. While DESs work well in the majority of cases (Byrne et al., 2015), their permanency is associated with delayed healing of the vessel and thrombosis risk, with most patients receiving an expensive and prolonged course of dual antiplatelet therapy (Byrne et al., 2015). Moreover, if in-stent restenosis (ISR) occurs, it is not feasible to remove the original stent and insert a new one, which complicates the repeat revascularisation strategy.

Drug-coated balloons (DCBs) have emerged as an attractive alternative to DESs for the treatment of CAD in certain anatomical conditions. In particular, DCBs may be used in the treatment of ISR, where it is not feasible to insert a further DES (Scheller et al., 2006). Moreover,

* Corresponding author at: Division of Biomedical Engineering, University of Glasgow, Glasgow, UK.
E-mail address: sean.mcginty@glasgow.ac.uk (S. McGinty).

https://doi.org/10.1016/j.ijpharm.2022.121742
Received 26 February 2022; Received in revised form 3 April 2022; Accepted 8 April 2022
Available online 12 April 2022

DCBs are becoming increasingly interesting in the context of treating small de novo lesions (Jeger et al., 2018). A key potential advantage of deploying a DCB over a DES is the lack of permanency. However, this may potentially be a disadvantage, where the brief period of deployment associated with DCBs presents only a short window for drug to be delivered. Specifically, while DCBs typically transfer drug rapidly to the arterial wall during a short application period of the order of 1 min (Cortese and Bertoletti, 2011; Heilmann et al., 2010), DESs usually offer sustained drug release over a period of weeks or months. It is therefore of interest to explore how the different time scales of delivery between DCBs and DESs influence drug delivery and retention. Current commercial DESs almost exclusively elute limus compounds (Lee and Torre Hernandez, 2018). While the first DCBs eluted paclitaxel (Scheller et al., 2006), thought to be advantageous given the short drug delivery window (Bozsak et al., 2014), more recent efforts have considered different formulations of limus-eluting balloons (e.g. utilising nanoparticle technology) (Sojitra et al., 2013). How the differing physico-chemical properties of these commonly used compounds influences the success of DCB treatment remains to be resolved (McQueen et al., 2021).

Mathematical and computational modelling has emerged as a powerful tool to simulate drug release from medical devices and subsequent transport in the biological environment. In particular, there is rich literature on mathematical and computational modelling of DESs (McGinty, 2014). Such analysis has uncovered that stent drug kinetics are governed by physiological transport forces (diffusion and advection) (Hwang et al., 2001), arterial ultrastructures (Hwang and Edelman, 2002) and the drug physicochemical properties (Hwang et al., 2003). These early studies provided mechanistic explanations for the superior results that were observed with stents coated with lipophilic vs hydrophilic compounds, while more recent work has highlighted the importance of including two phases of nonlinear drug binding (specific and non-specific) within the models (Tzafriri et al., 2009; Tzafriri et al., 2012; McKittrick et al., 2019), with saturation of specific receptors being strongly linked to efficacy, at least for sirolimus-eluting stents. It is notable that, despite the complex physics and biology that underpins these models, they were simplified in the sense that they considered only one spatial dimension. The most advanced models of DES kinetics now include multiple layers of the arterial wall in more realistic, but still idealised, 2D-axisymmetric models (Escuer et al., 2021).

Despite the plethora of models that consider DESs, there are only a handful of mathematical and computational models that focus on DCBs (Kolachalama et al., 2013; Mandal et al., 2016; Sarifuddin and Mandal, 2018; Tzafriri et al., 2019; Anbalakan et al., 2021; Colombo et al., 2021; Jain et al., 2022), each with their own set of strengths and limitations (Table 1). Commonalities between these models include the assumptions that drug is transported by diffusion within the arterial wall and that drug binding plays a key role in drug distribution and retention. However, the level of complexity of the binding model, the influence of other transport processes such as advection, and how the drug source is incorporated, is handled differently between the models. Moreover, the models range from 1D to 3D and while some incorporate disease (either heterogeneous (Sarifuddin and Mandal, 2018) or homogeneous (Anbalakan et al., 2021; Colombo et al., 2021)), some do not. The only existing model that incorporates the multilayer nature of the arterial wall has very recently been presented by (Jain et al., 2022). However, their primary goal was to provide an analytical solution, necessitating simplifications in other aspects (dimensionality and linearity of the binding model).

In this paper we present the most comprehensive model of DCB delivery, transport and retention to date. We employ a 2D-axisymmetric geometry, incorporate two nonlinear phases of binding (specific and non-specific) and include the influence of advection, within a multilayer arterial wall. We utilise this framework to (i) simulate drug delivery from different types of balloon platform (Kolachalama et al., 2013; Anbalakan et al., 2021); (ii) explore the influence of DCB application time; (iii) elucidate the importance on release kinetics of elevated pressure during DCB application; (iv) compare DCB delivery of two different drugs (sirolimus [SIR] and paclitaxel [PTX]) and; (v) compare simulations of DESs vs DCBs to explore if there are any potential benefits, in terms of safety and efficacy, of treating small de novo lesions with a DCB vs a DES.

2. Methodology

2.1. Geometrical model

We consider two different 2D-axisymmetric geometries corresponding to idealised straight sections of coronary arteries where either a DCB is deployed or a DES with non-erodible polymeric coating is implanted (Fig. 1). In each case, a lesion length of 7 mm is assumed (Bozsak et al., 2014), while we calculate drug concentrations within an extended therapeutic domain of 10.5 mm in length. A three-layer arterial wall is considered, including the subendothelial space (SES), media and adventitia.

To model drug delivery from a DCB, we impose a flux condition on the lumen-tissue interface across the lesion, while drug delivery from a DES is assumed to occur from ten struts half-embedded in the arterial wall (Bozsak et al., 2014; Escuer et al., 2021). Drug transport within the arterial wall is governed by advection-diffusion-reaction equations, which we parameterise on a layer-specific basis. It is noteworthy that the flow field within the porous tissue is governed by Darcy's law, driven by the pressure gradient between the lumen and the perivascular tissue. In existing state-of-the-art models of drug kinetics following stenting (Bozsak et al., 2014; Escuer et al., 2020; Escuer et al., 2021), the pressure in the lumen is commonly calculated by solving the steady Navier–Stokes and continuity equations, while drug transport within the lumen is typically modelled through an advection–diffusion equation. Under these conditions, our preliminary simulations (See Supplementary Material S1) indicated that the pressure along the lumen-wall interface is approximately constant. Moreover, they indicated that advection–diffusion of drug within the lumen leads to essentially zero drug concentration in the lumen. In other words, the lumen effectively acts as

Table 1
Summary of the existing models of DCB kinetics, highlighting key considerations and limitations.

Reference	Drug source	Binding model	Advection included?	Disease included?	Dimension	Multilayer?
Kolachalama et al., 2013	Flux	One phase, nonlinear	No	No	2D	No
Sarifuddin and Mandal, 2018	Flux	One phase, nonlinear	Yes	Yes	2D	No
Tzafriri et al., 2019	Flux	Two phases, nonlinear	No	No	1D	No
Anbalakan et al., 2021	Flux	Two phases, nonlinear	Yes	Yes	2D	No
Colombo et al., 2021	Constant	One phase, nonlinear	No	Yes	3D	No
Jain et al., 2022	Constant	One phase, linear	Yes	No	1D	Yes

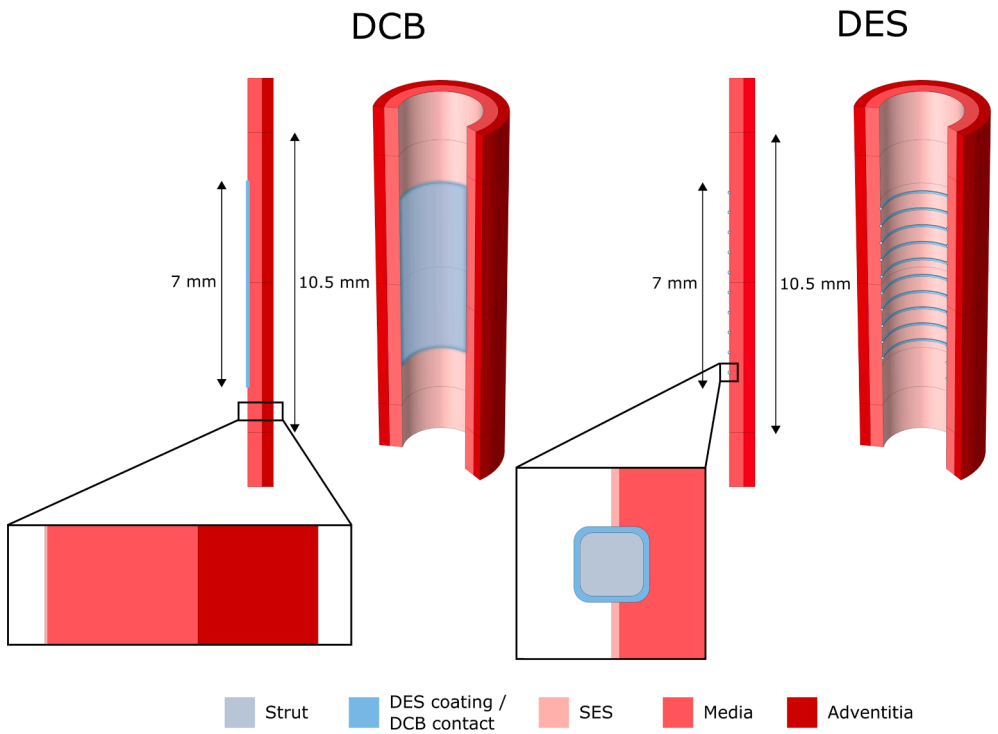

Fig. 1. Schematic summarising the geometric model employed for the DCB (left) and the DES (right). SES: subendothelial space. In each case, a lesion length of 7 mm is assumed, while we calculate drug concentrations within an extended therapeutic domain of 10.5 mm in length.

a sink for drug. Taken together, these findings allow us to significantly reduce the complexity of the model: through symmetry, we only need to solve our model equations on half the arterial wall domain. The pressure calculated from our preliminary simulations is used to define the pressure gradient (and consequently the advective term) in Darcy's law, while an infinite sink condition is assumed for drug in contact with the lumen.

2.2. Governing equations

2.2.1. Modelling drug release from the DCB and DES

We adopt two distinct approaches to modelling drug release from the DCB and the DES. As observed in Table 1, existing models of drug delivery from DCBs either prescribe a flux at the lumen-tissue interface or impose a constant drug concentration for the duration of balloon application. During the period of balloon application ($t \leqslant t_0$) we adopt the former approach, utilising two different flux expressions from the literature that have been parameterised on experimental data. The first is provided by (Kolachalama et al., 2013) who considered a zotarolimus-eluting balloon, while the second is provided by (Anbalakan et al., 2021) who considered a sirolimus-eluting balloon. The same expression is used to describe the flux, J_{DCB}, in each case,

$$J_{DCB} = \frac{kA}{M_w}\exp(-kt), \quad t \leqslant t_0, \tag{1}$$

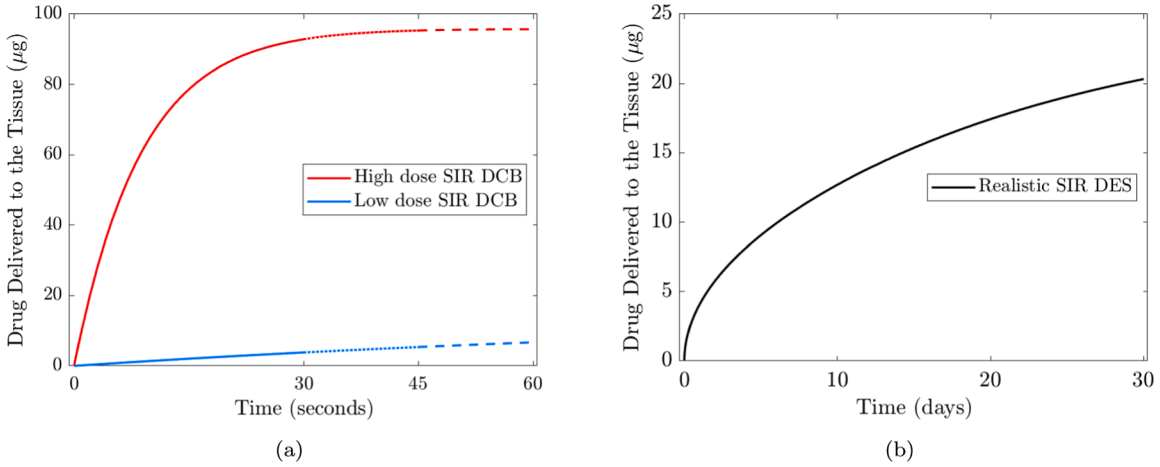

Fig. 2. Drug mass delivered to the arterial wall (a) Low dose and high dose sirolimus (SIR) DCB delivery, showing 30 s, 45 s and 60 s application times (different line styles). Simulations employ Eq. 1 with $k = 0.009221$ s^{-1}, $A = 0.24$ μg/mm^2 for the low dose flux expression (Kolachalama et al., 2013) and $k = 0.1135$ s^{-1}, $A = 1.4618$ μg/mm^2 for the high dose flux expression (Anbalakan et al., 2021). (b) SIR delivered to tissue from a realistic DES based on XIENCE V® (Abbott Laboratories, Abbott Park, IL, USA) drug release kinetics, with total drug loading of $M^0_{DES} = 50$ μg, strut thickness of 81μm, coating thickness of $L_{poly} = 8$ μm and drug coating diffusion coefficient of $D_{DES} = 1.5 \times 10^{-17}$ m^{2}s^{-1}.

where k and A are empirically estimated constants, M_w is the molecular weight of the drug and t is the time. Whilst the same form of expression is used, the inferred parameter values are quite different, resulting in a substantial difference in the overall influx of drug. To effect comparison between the respective flux expressions, we assume k and A are drug-independent and utilise the molecular weight, M_w, of sirolimus in Eq. 1. The mass of drug delivered to the tissue over 60 s is then found to vary from 6.7 μg to 96.3 μg using the (Kolachalama et al., 2013) and (Anbalakan et al., 2021) fluxes, respectively (Fig. 2a). This discrepancy is likely due to the differing excipients used (proprietary and polyethylene oxide, respectively) and, to a lesser extent, the physicochemical properties of the drugs. While both the mass of drug delivered and the shape of the flux vary, for the remainder of this paper we refer to the flux expression provided by (Kolachalama et al., 2013) as *low dose* while we refer to the flux expression provided by (Anbalakan et al., 2021) as *high dose*.

Following balloon removal ($t > t_0$), the flux boundary condition (1) is replaced with a sink boundary condition for drug ($c_{DCB} = 0$), to be consistent with our observation (see Supplementary Material S1.3) that any drug at the lumen-wall interface is washed away by the blood. Note that the imposition of such a boundary condition assumes that balloon coating adherence to the tissue is negligible, since this would potentially act as a reservoir for more sustained drug release. Such a mechanism has been reported in the literature for certain drug/excipient combinations (Chang et al., 2019; Tzafriri et al., 2020).

In line with the existing literature (McGinty, 2014), drug release from a DES with non-erodible polymeric coating is modelled as a diffusion dominated process satisfying a linear diffusion equation:

$$\frac{\partial c_{DES}}{\partial t} = \nabla\cdot(D_{DES}\nabla c_{DES}), \tag{2}$$

where $c_{DES}\ (r, z, t)$ is the volume-averaged concentration of drug within the stent coating and D_{DES} represents the effective drug diffusion coefficient within the polymer, assumed to be constant and isotropic. At $t = 0$, the drug is assumed to be completely contained within the polymer coating in dissolved phase (free drug) at uniform concentration, C_0, derived from the drug loading mass. The strut shape, strut thickness, coating thickness L_{poly}, drug mass loading M^0_{DES} and drug diffusion coefficient (Fig. 2b) are based upon XIENCE V® (Abbott Laboratories, Abbott Park, IL, USA) which releases approximately 80% of its drug load within 30 days (Perkins et al., 2009).

2.2.2. Modelling drug transport within the arterial wall

The arterial wall is modelled as a multilayered structure organised in three porous layers: SES, media and adventitia. Due to the porous nature of the tissue, the flow field through the different regions of the arterial wall is calculated using Darcy's law and the continuity equation:

$$\boldsymbol{u}_i = \frac{K_i}{\mu_p}\nabla p_i,\ \ \nabla\cdot\boldsymbol{u}_i = 0, \tag{3}$$

where the subscript $i = \{ses, m, a\}$ denotes the SES, the media and the adventitia, respectively; $\boldsymbol{u}_i$ is the transmural velocity vector field; K_i is the Darcian permeability; μ_p is the dynamic viscosity of the plasma; and p_i is the pressure field. The endothelium (ET), internal and external elastic laminae (IEL and EEL, respectively) are treated as semipermeable membranes and the fluid flux across them, $J_{v,j}$, is described by the Kedem-Katchalsky equations (Kedem and Katchalsky, 1958). Neglecting the osmotic contribution as an approximation (Formaggia et al., 2010; Bozsak et al., 2014; Bozsak et al., 2015; Escuer et al., 2020; Escuer et al., 2021), the Kedem-Katchalsky equations for fluid flux can be simplified as:

$$J_{v,j} = L_{p,j}\Delta p_j, \tag{4}$$

where the subscript $j = \{et, iel, eel\}$ denotes the endothelium (lumen-SES interface), the internal elastic lamina (SES-media interface) and the external elastic lamina (media-adventitia interface), respectively; $L_{p,j}$ is the membrane hydraulic conductivity and; Δp_j the pressure drop across each semipermeable membrane. The equations for the flux J_v, corresponding to each boundary, are shown in the Supplementary Material (S2).

Due to DCB and DES deployment, the endothelium is assumed to be denuded across the lesion length of 7 mm and, in the case of the DES, between struts and a distance corresponding to half of the interstrut spacing (ISS) proximal and distal to the lesion (Bozsak et al., 2014). Outside of these regions the endothelium is assumed to be intact. In denuded regions, the volume flux across the endothelium simplifies to continuity of pressure, i.e. $p_l = p_{ses}$, where the subscript l denotes the lumen. Upstream of the lesion, we impose a zero-flow condition at the longitudinal boundaries, $U_i := -\boldsymbol{n}_i\cdot\boldsymbol{u}_i = 0$, where $\boldsymbol{n}_i$ is the unit outward normal vector to the corresponding exterior boundary, in agreement with previous studies (Bozsak et al., 2014; Escuer et al., 2020). This choice of boundary condition is justified by the fact that we are interested in computing drug concentrations only within the therapeutic domain while these boundaries are imposed sufficiently far upstream and downstream of the lesion. Similar conditions are applied at the axis of symmetry at the midpoint of the lesion. Moreover, it is assumed that the plasma cannot penetrate the surface of the DES polymer coating. At the lumen and perivascular tissue, constant pressures of 100 mmHg (derived from our prelimary simulations, see Supplementary Material S1.3) and 30 mmHg (Ai and Vafai, 2006) are considered, emulating a physiologically realistic pressure drop of 70 mmHg (Meyer et al., 1996). However, during the period of DCB inflation ('*inf*'), we consider an increased pressure of $p_{inf} = 8$ atm (Anbalakan et al., 2021) across the denuded region, corresponding to the pressure at which balloons are typically inflated during angioplasty:

$$p_{ses} = \begin{cases} p_{inf}, & t \leqslant t_0 \\ p_l, & t > t_0. \end{cases} \tag{5}$$

Drug transport within the SES and the adventitia may be written as advection–diffusion equations:

$$\frac{\partial c_{ses}}{\partial t} + \frac{\gamma_{ses}}{\phi_{ses}}\boldsymbol{u}_{ses}\cdot\nabla c_{ses} = \nabla\cdot(\boldsymbol{D}_{ses}\nabla c_{ses}), \tag{6}$$

$$\frac{\partial c_a}{\partial t} + \frac{\gamma_a}{\phi_a}\boldsymbol{u}_a\cdot\nabla c_a = \nabla\cdot(\boldsymbol{D}_a\nabla c_a). \tag{7}$$

The parameters $\gamma, \phi, \boldsymbol{u}, \boldsymbol{D}$ and $c(r, z, t)$ refer to the hindrance coefficients, porosities, transmural fluid velocities calculated by Eq. (3), diffusivity tensors and dissolved drug concentrations within the respective domains. Within the media, in addition to advection and diffusion, drug binding processes are thought to strongly influence drug transport and retention. Therefore, we incorporate state-of-the-art two-phase nonlinear saturable binding kinetics, distinguishing between drug bound specifically to target receptors (s) and non-specifically to extracellular matrix (ECM) components (ns). The resulting advection–diffusion-reaction equation within the media is:

$$\frac{\partial c_m}{\partial t} + \frac{\gamma_m}{\phi_m}\boldsymbol{u}_m\cdot\nabla c_m = \nabla\cdot(\boldsymbol{D}_m\nabla c_m) - \frac{\partial b^{ns}_m}{\partial t} - \frac{\partial b^{s}_m}{\partial t}, \tag{8}$$

$$\frac{\partial b^{ns}_m}{\partial t} = k^{ns}_{on}c_m(b^{ns}_{max,m} - b^{ns}_m) - k^{ns}_{off}b^{ns}_m, \tag{9}$$

$$\frac{\partial b^{s}_m}{\partial t} = k^{s}_{on}c_m(b^{s}_{max,m} - b^{s}_m) - k^{s}_{off}b^{s}_m, \tag{10}$$

where $b^s_m(r, z, t)$ and $b^{ns}_m(r, z, t)$ denote the concentration of drug bound specifically and non-specifically, with respective binding on and binding off rates given by $k^s_{on}, k^{ns}_{on}, k^s_{off}$ and k^{ns}_{off}. The parameters $b^s_{max,m}, b^{ns}_{max,m}$ denote, respectively, the maximum density of specific and non-specific

binding sites within the media. Discontinuity of solute flux across the semipermeable membranes, $J_{s,j}$, is governed by the Kedem-Katchalsky equations (Kedem and Katchalsky, 1958):

$$J_{s,j} = P_j \Delta c_j + s_j \bar{c}_j J_{v,j} \tag{11}$$

where P_j is the permeability of each semipermeable membrane; Δc_j is the solute concentration difference; s_j is the sieving coefficient and; $\bar{c}_j$ is the weighted average concentration on either side of the corresponding membrane (Levitt, 1975). The equations for the flux J_s corresponding to each boundary are shown in the Supplementary Material (S2). The upstream tissue boundary (Vairo et al., 2010) and symmetry plane at the centre of the lesion are subjected to zero-flux conditions: $N_i := -\boldsymbol{n}_i \cdot (-\boldsymbol{D}_i \nabla c_i + \boldsymbol{u}_i c_i) = 0$. A perfect sink condition for the free drug is applied at the perivascular side, $c_a = 0$ (Bozsak et al., 2014; Escuer et al., 2020) and in the case of the DES also at the lumen, $c_{ses} = 0$. In the case of the DES, continuity of drug concentration and mass flux is prescribed across the outer boundary of the polymeric stent coating:

$$c_{DES} = c_k, \tag{12}$$

$$J_{s,DES} = \left(-\boldsymbol{D}_{DES} \nabla c_{DES}\right) \cdot \boldsymbol{n}_{DES} = -\left(-\boldsymbol{D}_k \nabla c_k + \boldsymbol{u}_k c_k\right) \cdot \boldsymbol{n}_k, \quad k = \{ses, m\}. \tag{13}$$

Finally, we assume a perfect sink at the interface between the stent struts and the lumen ($c_{DES} = 0$) and that the metallic DES struts are imper-

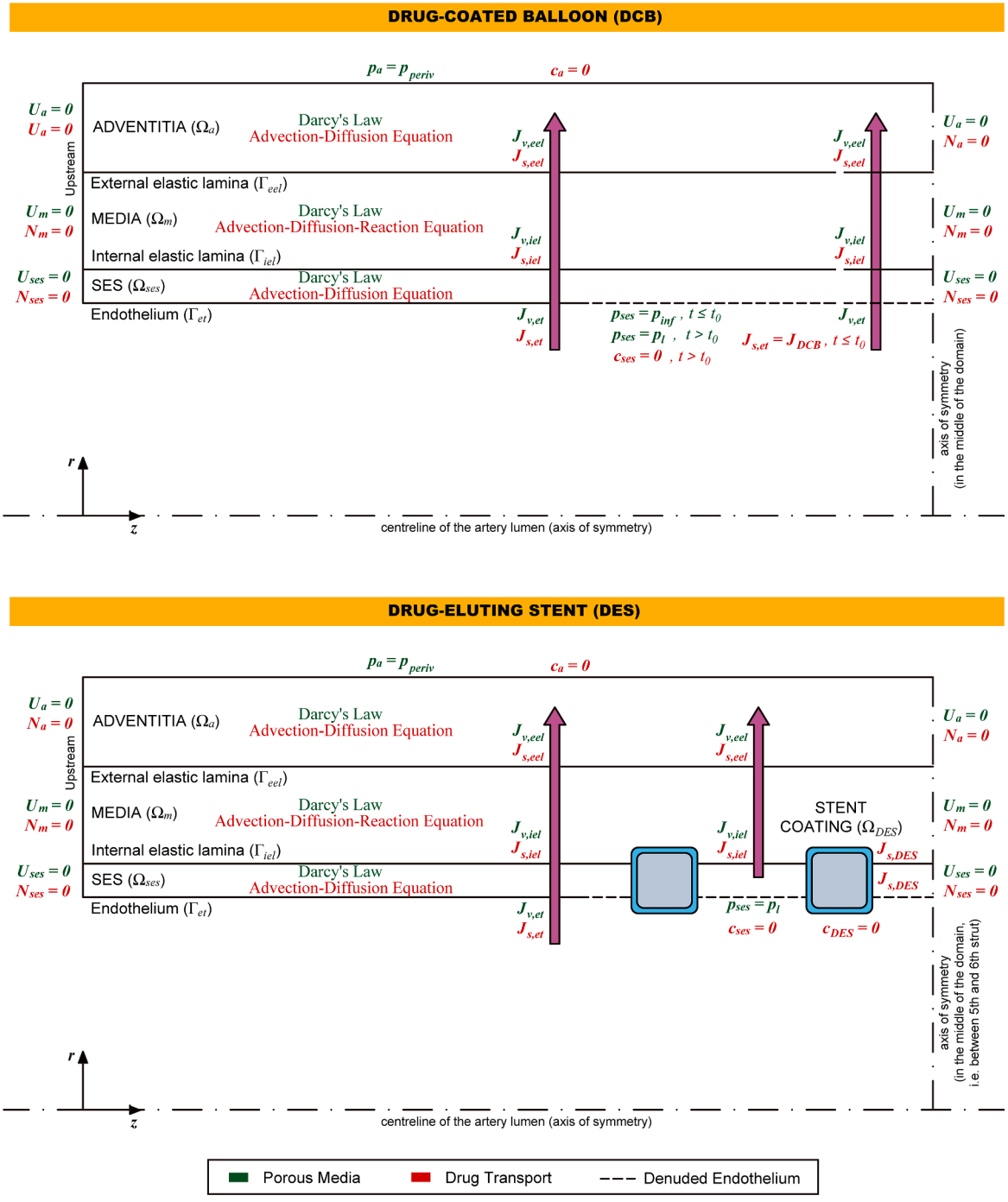

Fig. 3. Schematic summarising the governing equations and boundary conditions involved in the computational models of DCB and DES drug delivery. For notation, please refer to the main text.

meable to the drug ($-\boldsymbol{n}_{DES}\cdot(-D_{DES}\nabla c_{DES}) = 0$). We refer the reader to Fig. 3 for a schematic summarising the governing equations and boundary conditions involved in the computational models of DCB and DES drug delivery.

2.3. Numerical methods

The commercial finite element (FE) package COMSOL Multiphysics 5.6 (COMSOL AB, Burlington, MA, USA) was used to build the mesh and to numerically solve the governing equations described in Section 2 for the different cases considered. The computational analysis for the DCB

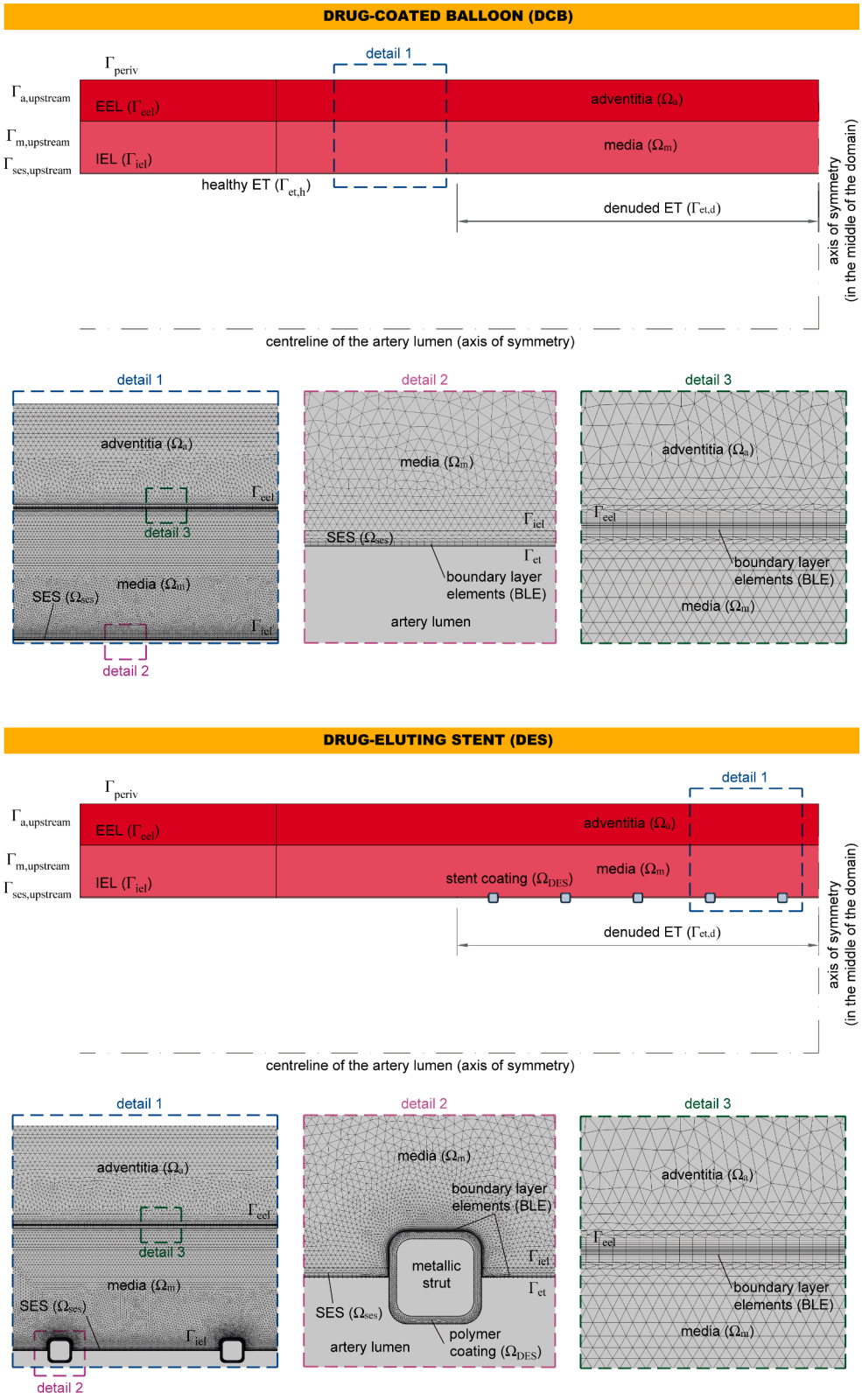

Fig. 4. Detailed view of the Finite Element mesh used in the computations. For notation, please refer to the main text.

Table 2
Summary of the different cases considered. (*) denotes the initial drug loading considering the full domain.

Case	Name	Device	Drug	J_{DCB}	D_{DES}	M^0_{DES}	Coating thickness
1	Low Dose SIR DCB	DCB	Sirolimus	Low dose	n/a	n/a	n/a
2	High Dose SIR DCB	DCB	Sirolimus	High dose	n/a	n/a	n/a
3	Low Dose PTX DCB	DCB	Paclitaxel	Low dose	n/a	n/a	n/a
4	Realistic SIR DES	DES	Sirolimus	n/a	1.5×10^{-17} m^2s^{-1}	50 μg (*)	8 μm
5	Fast SIR DES	DES	Sirolimus	n/a	1×10^{-13} m^2s^{-1}	96.3 μg (*)	1.456 μm

cases was conducted in four steps: (1) a stationary analysis of the plasma filtration during inflation; (2) a time-dependent drug transport analysis coupled with the solutions of transmural flow computed in the previous step; (3) a stationary analysis of the plasma filtration post-angioplasty; and (4) a time-dependent drug transport analysis coupled with the solutions of transmural flow computed in the previous step. The computational analysis for the DES cases was conducted in two steps: (1) a stationary analysis of the plasma filtration; (2) a time-dependent drug transport analysis coupled with the solutions of transmural flow computed in the previous step. A sensitivity analysis was carried out in order to evaluate the influence of the mesh and time-step size on the solution. Mesh density and time-step independence was assumed when there was less than 1% difference in the time varying profiles of drug content in the tissue after several mesh and time-step refinements. The computational domains were discretized in space using triangular elements, resulting in an overall mesh varying between approximately 128000 and 594000 elements for the DCB models and between 158000 and 300000 elements for the DES models. The triangular mesh was enhanced with boundary layer elements (BLE) at the endothelium and the external elastic lamina for both DES and DCB cases and, moreover, at the interface of the stent polymeric coating with the tissue for DES cases, in order to smooth the sharp initial condition between the stent polymer and the surrounding domain. The spatial discretization employs quadratic Lagrange elements for the porous media and drug dynamics problems, respectively. Details of the mesh used in the different regions of the computational models are illustrated in Fig. 4.

A Multifrontal Massively Parallel Sparse (MUMPS) direct solver was used to solve the stationary steps with a tolerance for the relative error of the solution of 10^{-3}. The backward differentiation formula (BDF) method was used for the time discretization of the transient steps, with variable order of accuracy between 1 and 5 and variable time-step size, with the maximum time-step size restricted to 1 h. The relative and absolute tolerance was set to 10^{-3} and 10^{-4}, respectively. The resulting system of time-dependent partial differential equations (PDEs) was

Table 3
List of model parameters related to the arterial tissue.

Parameter	Description	Value	Reference
r_l	Lumen radius	1.5 mm	Mongrain et al., 2005
δ_{ses}	Intima thickness	0.01 mm	Karner et al., 2001
δ_m	Media thickness	0.5 mm	Vairo et al., 2010
δ_a	Adventitia thickness	0.4 mm	Creel et al., 2000
p_l	Pressure in the lumen	100 mmHg	Ai and Vafai, 2006
p_{inf}	Pressure during DCB application	8 atm	Anbalakan et al., 2021
p_{periv}	Pressure in the perivascular tissue	30 mmHg	Ai and Vafai, 2006
ρ_p	Plasma density	1060 kg m^{-3}	Bozsak et al., 2014
μ_p	Plasma dynamic viscosity	$7.2 \cdot 10^{-4}$ Pa s	Zunino, 2004
ϕ_{ses}	Porosity of the intima	0.983	Ai and Vafai, 2006
ϕ_m	Porosity of the media	0.258	Ai and Vafai, 2006
ϕ_a	Porosity of the adventitia	0.85	Lovich and Edelman, 1996
γ_{ses}	Hindrance coefficient in the intima	1	Escuer et al., 2020
γ_m	Hindrance coefficient in the media	0.845	Escuer et al., 2020
γ_a	Hindrance coefficient in the adventitia	1	Escuer et al., 2020
κ_{ses}	Darcy permeability in the intima	$2.2{\cdot}10^{-16}$ m^2	Ai and Vafai, 2006
κ_m	Darcy permeability in the media	$2{\cdot}10^{-18}$ m^2	Zunino, 2004
κ_a	Darcy permeability in the adventitia	$2{\cdot}10^{-18}$ m^2	Vairo et al., 2010
$L_{p,et}$	Hydraulic conductivity of endothelium	$2.2{\cdot}10^{-12}$ m^2 s kg^{-1}	Bozsak et al., 2014
$L_{p,iel}$	Hydraulic conductivity of IEL	$2.2{\cdot}10^{-9}$ m^2 s kg^{-1}	Bozsak et al., 2014
$L_{p,eel}$	Hydraulic conductivity of EEL	$2.2{\cdot}10^{-9}$ m^2 s kg^{-1}	Escuer et al., 2020
ρ	Density of wet arterial tissue	0.983 g ml^{-1}	Tzafriri et al., 2012

solved using a Parallel Direct Sparse Solver (PARDISO). Using14 cores of an Intel® Core™ i9-10940X CPU @ 3.30 GHz processor, the computation time for each of the simulations carried out varied between 2 and 19 h.

2.4. Summary of investigated cases

We simulate 5 distinct cases covering DCBs with different drug delivery kinetics, drug doses and drug types and DESs with different drug release kinetics. The various cases considered are summarised in Table 2. Case 5 represents an 'artificial' stent where we have adjusted the drug diffusion coefficient in the stent coating and coating thickness to match the mass of drug delivered by 60 s with Case 2 (the high dose SIR DCB). The purpose of simulating Case 5 is to establish if, in principle, it would be possible to design a DES with similar release kinetics to the DCB.

2.5. Analysis of the results

In order to facilitate comparison between the various cases simulated (Table 2) we calculate three time-dependent quantities of interest over a period of 30 days. Firstly, drug content (*DC*) quantifies μg drug/g tissue and is a key measure of safety. The *DC* is given by:

$$DC(t) = \sum_i \frac{M_w}{\rho V_i} \int_{V_i} \left(c_i + b_i^s + b_i^{ns}\right) dV_i, \tag{14}$$

where V_i denotes the volume of layer i and ρ is the density of wet arterial tissue. Plotting *DC* over time allows visualisation of the peak drug concentration in the tissue and the time at which this occurs, as well as indicating the ability of the tissue to retain the drug. Secondly, since sustained saturation of specific binding sites (% *SBSS*) has been strongly linked with efficacy (Tzafriri et al., 2012; McKittrick et al., 2019) we compute this quantity via:

$$\%SBSS(t) = \frac{100}{V_m \cdot b_{max,m}^s} \int_{V_m} b_m^s dV_m. \tag{15}$$

Finally, while not directly indicative of safety or efficacy, non-specific binding site saturation (% *NSBSS*) is also computed since it contributes to drug retention within the tissue:

Table 4
List of model parameters related to the different drugs considered: sirolimus (SIR) and paclitaxel (PTX).

Parameter	Description	Value SIR	Value PTX	Ref.
D_{ses}	Effective diffusion coefficient in the intima	$1.67{\cdot}10^{-11}$ m^2 s^{-1}	$1.70{\cdot}10^{-11}$ m^2 s^{-1}	Bozsak et al., 2014
$D_{m,r}$	Effective radial diffusion coefficient in the media	$7{\cdot}10^{-12}$ m^2 s^{-1}	$2{\cdot}10^{-12}$ m^2 s^{-1}	Levin et al., 2004
$D_{m,z}$	Effective axial diffusion coefficient in the media	$4{\cdot}10^{-11}$ m^2 s^{-1}	$5{\cdot}10^{-11}$ m^2 s^{-1}	Levin et al., 2004
D_a	Effective diffusion coefficient in the adventitia	$4{\cdot}10^{-12}$ m^2 s^{-1}	$4{\cdot}10^{-12}$ m^2 s^{-1}	Escuer et al., 2020
P_{et}	Permeability of ET	$3.6{\cdot}10^{-6}$ m s^{-1}	$3.0{\cdot}10^{-6}$ m s^{-1}	Bozsak et al., 2014
P_{iel}	Permeability of IEL	$9.6{\cdot}10^{-6}$ m s^{-1}	$9.8{\cdot}10^{-6}$ m s^{-1}	Bozsak et al., 2014
P_{eel}	Permeability of EEL	$9.6{\cdot}10^{-6}$ m s^{-1}	$9.6{\cdot}10^{-6}$ m s^{-1}	Escuer et al., 2020
s_{et}	Sieving coefficient in the ET	0.855	0.860	Bozsak et al., 2014
s_{iel}	Sieving coefficient in the IEL	1	1	Bozsak et al., 2014
s_{eel}	Sieving coefficient in the EEL	1	1	Escuer et al., 2020
K_d^{ns}	Non-specific equilibrium dissociation constant	$2.6{\cdot}10^{-3}$ mol m^{-3}	$3.1{\cdot}10^{-3}$ mol m^{-3}	Rami Tzafriri et al., 2009
k_{on}^{ns}	Non-specific drug binding rate constant	2 m^3 mol^{-1} s^{-1}	0.17 m^3 mol^{-1} s^{-1}	Rami Tzafriri et al., 2009; Escuer et al., 2020
k_{off}^{ns}	Non-specific drug unbinding rate constant	$5.2{\cdot}10^{-3}$ s^{-1}	$5.27{\cdot}10^{-4}$ s^{-1}	McGinty and Pontrelli, 2016; Escuer et al., 2020
$b_{max,m}^{ns}$	Non-specific binding site density in the media	0.363 mol m^{-3}	0.117 mol m^{-3}	Tzafriri et al., 2012; Rami Tzafriri et al., 2009; Díaz et al., 2003
K_d^s	Specific equilibrium dissociation constant	$2{\cdot}10^{-7}$ mol m^{-3}	$2.5{\cdot}10^{-5}$ mol m^{-3}	Bierer et al., 1990; Díaz et al., 2003
k_{on}^s	Specific drug binding rate constant	800 m^3 mol^{-1} s^{-1}	$3.6{\cdot}10^{-3}$ m^3 mol^{-1} s^{-1}	Wear and Walkinshaw, 2007; Díaz et al., 2003
k_{off}^s	Specific drug unbinding rate constant	$1.6{\cdot}10^{-4}$ s^{-1}	$9.1{\cdot}10^{-2}$ s^{-1}	McGinty and Pontrelli, 2016; Díaz et al., 2003
$b_{max,m}^s$	Specific binding site density in the media	$3.3{\cdot}10^{-3}$ mol m^{-3}	$1.0{\cdot}10^{-2}$ mol m^{-3}	Tzafriri et al., 2012; Díaz et al., 2003
M_w	Molecular weight	914.2 g mol^{-1}	853.9 g mol^{-1}	Levin et al., 2004

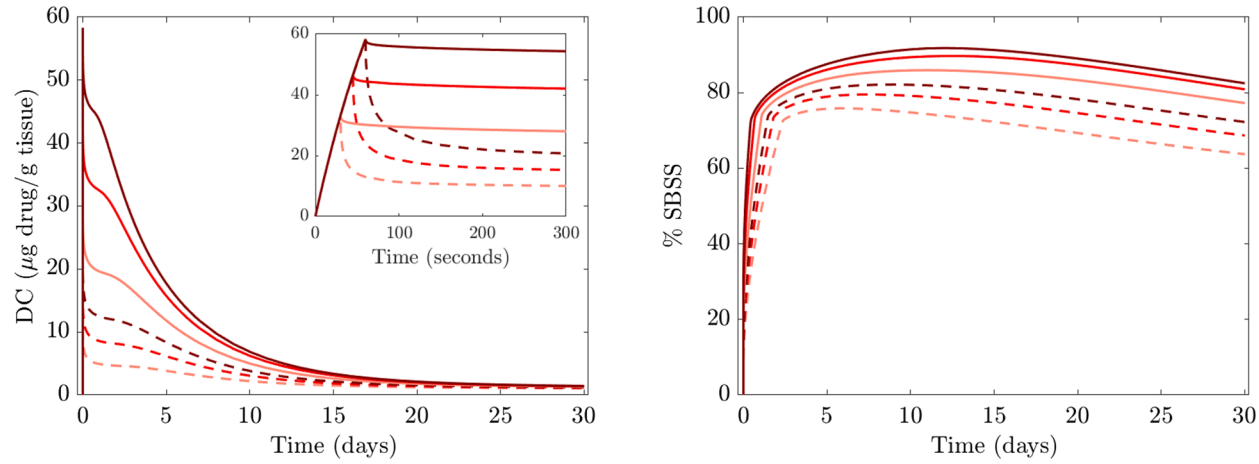

(a) Case 1: Low Dose SIR DCB

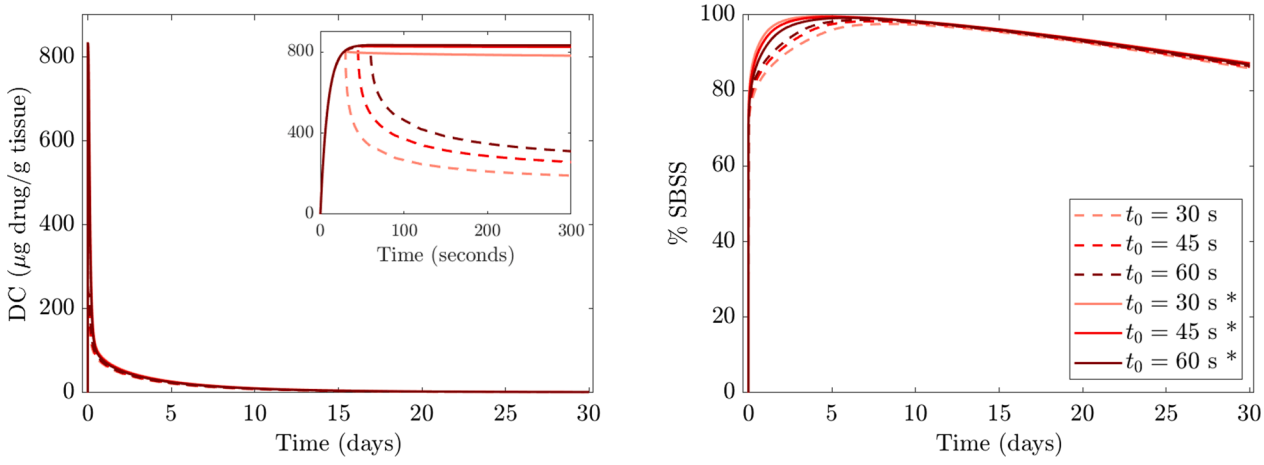

(b) Case 2: High Dose SIR DCB

Fig. 5. Comparison between (a) Case 1 (Low Dose SIR DCB) and (b) Case 2 (High Dose SIR DCB). LEFT: Drug Content (*DC*) vs time. RIGHT: % *SBSS* vs time. (*) denotes pressure increased over lesion to $p = p_{inf}$ for $t \leq t_0$ to match balloon inflation pressure.

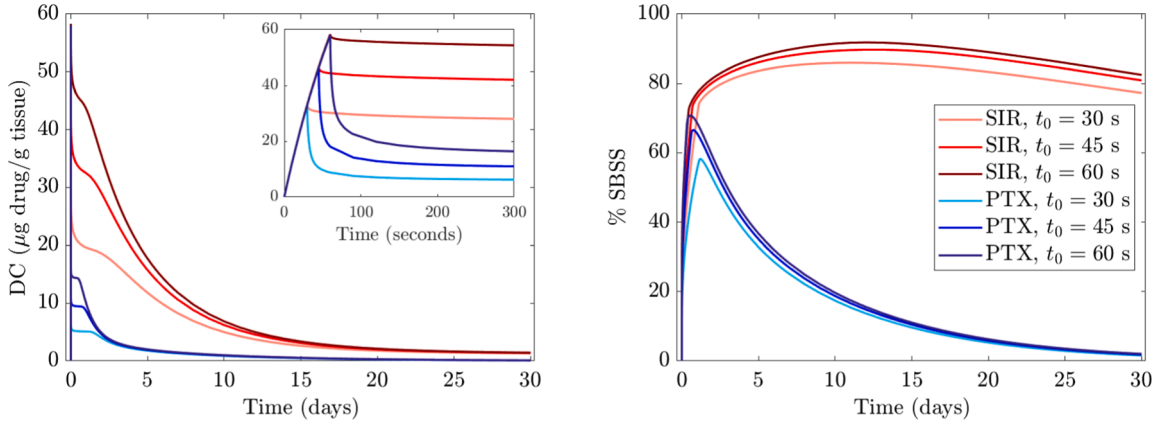

(a) (b)

Fig. 6. Comparison between Case 1 (Low Dose SIR DCB) and Case 3 (Low Dose PTX DCB). (a): Drug Content (*DC*) vs time. (b) % *SBSS* vs time. In all cases $p = p_{inf}$ for $t \leq t_0$ to match balloon inflation pressure.

$$\%NSBSS(t) = \frac{100}{V_m \cdot b^{ns}_{max,m}} \int_{V_m} b^{ns}_m dV_m. \quad (16)$$

In addition, we calculate spatial maps of drug distribution at 6 time points between 10 min and 30 days. The values of the various model parameters used in the simulations are included in Tables 3 and 4.

3. Results

3.1. Comparison between different DCB platforms

We start by comparing Case 1 with Case 2, i.e. deployment of SIR coated DCBs following either the low or high dose drug flux expression (Fig. 5a–b). In Fig. 5a (Left) we observe that for the low dose SIR DCB, as the balloon application time is increased, the peak *DC* increases since more drug is delivered to the arterial wall. This is true regardless of whether the lumen pressure for $t \leqslant t_0$ is simulated to be $p = 100$ mmHg or to match the balloon inflation pressure $p = p_{inf}$. However, it is notable that when $p = p_{inf}$ for $t \leqslant t_0$, *DC* declines substantially slower with time, in agreement with (Sarifuddin and Mandal, 2018). The rationale for this is that the increased advective term as a result of increased pressure gradient delivers drug deeper into the arterial wall, meaning that less drug is exposed to the lumen sink following balloon removal. This is more clearly observed in the spatial plots (Supplementary Fig. S2). This result indicates that it is imperative to incorporate the balloon inflation pressure within drug delivery simulations. The aforementioned trends are replicated when considering the high dose SIR DCB (Fig. 5b left). However, the corresponding peak *DC* values are substantially higher (greater than 10-fold) for the high dose SIR DCB compared with those achieved with the low dose SIR DCB and there is only a marginal difference in *DC* when extending the balloon application time from 30 −60 s for the high dose SIR DCB.

For the low dose SIR DCB, the majority of specific binding sites are saturated rapidly (within the first few days) in all cases considered (Fig. 5a right). The higher the DCB application time, the higher % *SBSS* is. Moreover, for the same reasons as described above, when $p = p_{inf}$ for $t \leqslant t_0$, higher % *SBSS* is achieved. This is echoed in the spatial plots of specific bound drug concentration (Supplementary Fig. S3). It is notable that after the early rapid increase in % *SBSS*, the rate of increase proceeds at a significantly slower rate, before reaching a peak and then declining approximately linearly with time over the remainder of the 30 days simulated: in the absence of a sustained source of drug delivery, drug unbinds and is cleared through the tissue via advection and diffusion, without being replenished. In Fig. 5b (right) we observe that the high dose SIR DCB leads to more rapid and higher levels of specific binding site saturation compared with the low dose SIR DCB. In particular, we note that approximately 95–100% *SBSS* is observed for all balloon application times considered. Moreover, the decline of % *SBSS* is slower than for the low dose SIR DCB. In other words, more receptors are saturated for longer with the high dose SIR DCB. Similarly to the low dose SIR DCB case, when $p = p_{inf}$ for $t \leqslant t_0$, higher % *SBSS* is achieved. For each case, %*NSBSS* follows a similar pattern to *DC*: the peak value is reached rapidly within the first day, before a quick decline to very low levels within approximately 15 days, indicating relatively rapid unbinding from non-specific binding sites (Supplementary Fig. S1a-S1b). In each case, %*NSBSS* is markedly lower than %*SBSS*, due to the larger density of non-specific binding sites compared with specific binding sites.

3.2. Comparison between DCBs coated with different drugs

In Fig. 6a–b we examine the influence of varying the drug delivered (either SIR or PTX) from the low dose DCB platform (Case 1 vs Case 3). Having already established the importance of accounting for the increased pressure during balloon inflation, all plots in Fig. 6a–b consider $p = p_{inf}$ for $t \leqslant t_0$. Since the mass of drug delivered is identical by definition, the *DC* peak is the same. However, the differing physiochemical properties of PTX gives rise to substantially quicker decline in *DC* levels within the arterial wall, compared with SIR (Fig. 6a). This is reflected in the % *SBSS* plot (Fig. 6b), where we observe lower peak specific receptor saturation values, and significantly faster decline of % *SBSS* for the PTX DCB compared with the SIR DCB. In other words, with the same delivery kinetics, in our simulations SIR is retained within the tissue for longer than PTX. This is a direct consequence of the differing physio-chemical properties of the drugs that we have obtained from the literature (we refer the reader to the Limitations section for discussion on this). In each case, there is a small increase in % *SBSS* with increased duration of balloon application. Regardless of which drug is used, % *NSBSS* never comes close to 100% saturation, reaching peaks of approximately 30% and 25% for the low dose SIR DCB and low dose PTX DCB, respectively (Supplementary Fig. S1c).

3.3. Comparison between DCB and DES

In Fig. 7a–b we compare the results for (i) the low dose SIR DCB; (ii) the high dose SIR DCB; (iii) the realistic SIR stent providing sustained drug release and; (iv) an artificial fast SIR stent whose properties have been tailored to match the drug influx from the high dose SIR DCB. As expected, we observe a significantly higher *DC* peak (greater than 10-fold) with the high dose SIR DCB and fast SIR DES compared with the

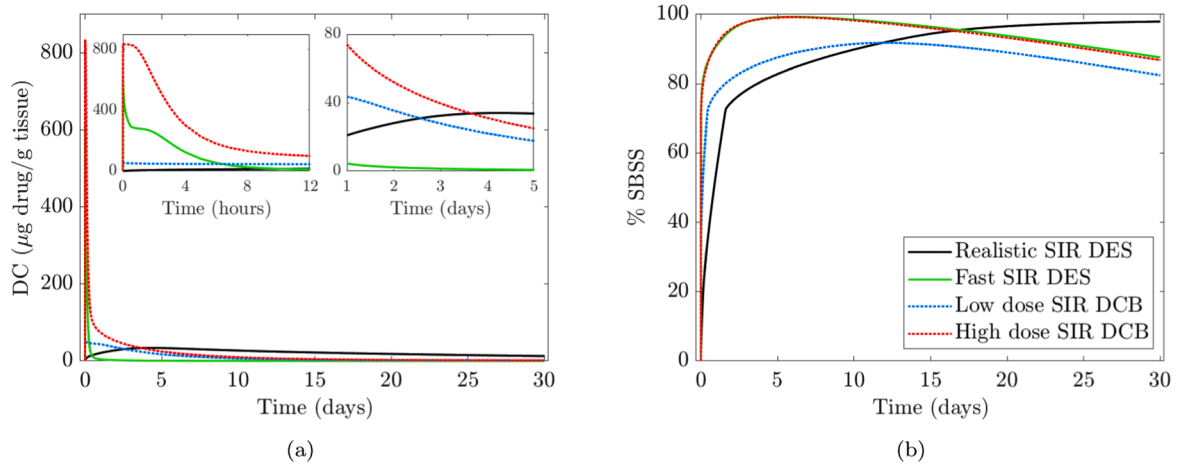

Fig. 7. Comparison between Case 1 (Low Dose SIR DCB), Case 2 (High Dose SIR DCB), Case 4 (Realistic SIR DES) and Case 5 (Fast SIR DCB). (a): Drug Content (*DC*) vs time. (b): % *SBSS* vs time. In all cases $p = p_{inf}$ for $t \leq t_0$ to match balloon inflation pressure.

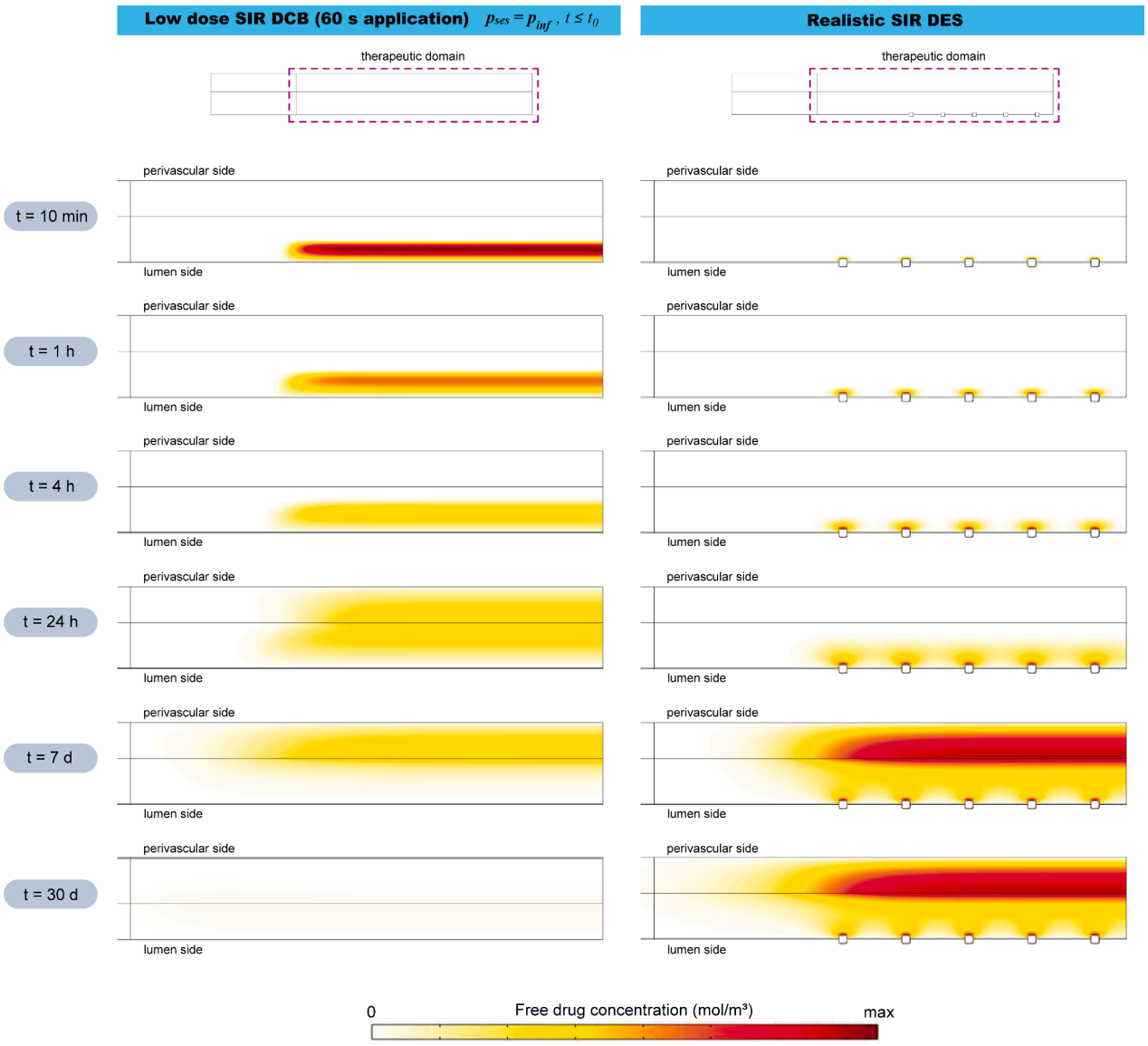

Fig. 8. Low dose SIR DCB vs realistic SIR DES spatial free drug concentration plots for $t = 10$ min, 1 h, 4 h, 24 h, 7 days and 30 days. For details of the max value in the scale, please refer to Table S1.

realistic SIR DES and the low dose SIR DCB (Fig. 7a). Moreover, the peak occurs earlier for the rapid delivery configurations (low dose SIR DCB, high dose SIR DCB, and fast SIR DES), compared with the more sustained release from the realistic SIR DES. Despite achieving a higher peak *DC*, the low dose SIR DCB, high dose SIR DCB and fast SIR DES result in rapid decline of *DC* to the extent that within a few days, they fall below the realistic SIR DES *DC* value and stay there for the remainder of the 30 days simulated. In other words, the realistic SIR DES results in a higher *DC* value for a greater portion of the 30 days. However, it is noted that, despite the similar drug influx from the high dose SIR DCB and fast SIR DES, the decline from the peak *DC* is notably slower for the high dose SIR DCB, likely as a consequence of the increased pressure during balloon application. It is enlightening to examine the spatial plots of free drug concentration for the low dose SIR DCB and the realistic SIR DES (Fig. 8). These plots highlight the rapid free drug delivery to the tissue, followed by relatively fast clearance through the tissue, for the DCB case compared with the slower and more sustained drug delivery of the DES. Also evident from these plots is the higher free drug concentrations at later times for the DES, with the DCB resulting in higher free drug concentrations at early times. Due to the heterogeneous delivery of drug in the case of the DES, free drug concentrations between struts remain very low for all times simulated. On the other hand, the homogeneous delivery of drug from the DCB ensures little axial variation in the free drug concentrations along the length of the lesion.

All cases considered achieve high levels of specific binding site saturation relatively rapidly, within the first day (approx. 75%–95%) (Fig. 7b). It is notable that the %*SBSS* curves of the high dose SIR DCB and fast SIR DES are almost identical, with each reaching higher values than the realistic SIR DES and the low dose SIR DCB. However, while the high dose SIR DCB and fast SIR DES achieve higher levels of % *SBSS* in the short term, with these levels declining steadily between approximately day 5 to day 30, the realistic SIR DES %*SBSS* level rises steadily over time, reaching approximately 100 % by 30 days. The spatial plots of specific bound drug concentration (Fig. 9) reflect these results. However, the spatial plots reveal that at later times, lower values of %*SBSS* for the case of the DCB are likely driven by lower drug concentrations at the lumen interface, as a direct result of the lack of a sustained drug source. With the exception of the realistic SIR DES, all cases considered rapidly reach their peak %*NSBSS* (of approximately 30 – 75%) before a decline to near negligible levels over a period of about 15 days (Supplementary Fig. S1d). In contrast, the realistic SIR DCB achieves a significantly lower %*NSBSS* peak of approximately 20%, which is

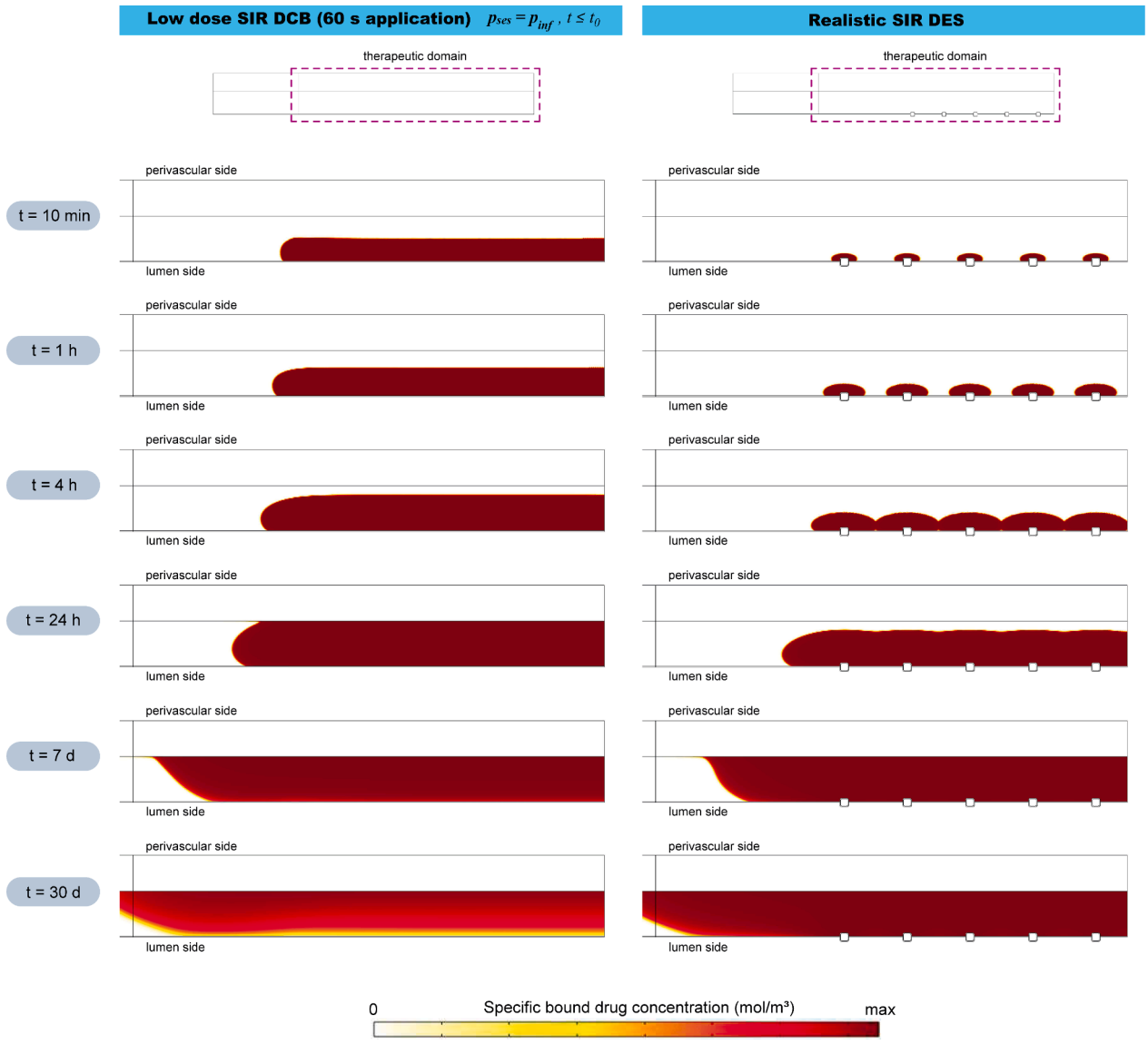

Fig. 9. Low dose SIR DCB vs realistic SIR DES spatial specifically bound drug concentration plots for $t = 10$ min, 1 h, 4 h, 24 h, 7 days and 30 days. For details of the max value in the scale, please refer to Table S1.

delayed with respect to the other cases (occurring at around day 5). However, %*NSBSS* declines at a substantially slower rate with values of around 8 −20% maintained for the remainder of the 30 days simulated.

3.4. Limitations

We wish to emphasise that, like all computational studies, there are a number of simplifications in this work. We reiterate that we have employed a simplified 2D-axisymmetric geometry which does not account for the presence of an atherosclerotic lesion, whose geometry and composition will vary from patient-to-patient. Moreover, tissue deformation as a result of DCB or DES deployment has not been considered. In our preliminary simulations, we employed the fluid dynamics equations that are typically used within the context of endovascular device drug transport simulations. In reality, blood does not always behave as a Newtonian fluid, and pulsatile flow would be a more accurate description than steady-flow. Notwithstanding, each of these features, which introduce additional complexity, have previously been shown to have a limited influence on drug concentrations within the arterial wall. We have gleaned parameter values from across the (large) literature in this field, the limitations of which we have previously discussed (Escuer et al., 2021). In particular we note that while a full set of binding parameters are available for SIR (Tzafriri et al., 2012), we have not been able to locate within the literature a full set of binding parameters (specific and non-specific) for PTX and have, therefore, been forced to calculate these from different sources. Regardless of the drug in question, to the best of our knowledge, there is no experimental data available in the literature that would allow one to impose different binding site densities within the different layers of the arterial wall. We further wish to reiterate that our model assumes that a negligible amount of DCB coating adheres to the arterial wall during application. If a sizeable portion of the coating adheres to the tissue, a feature likely to be highly dependent on the excipient/drug formulation, then this may act as a reservoir that would allow drug to be delivered to the arterial wall for far longer than the DCB application time. Finally, a key assumption underlying our model is that vessel wall remodelling does not significantly influence the transport and distribution of drug.

4. Discussion

DCBs and DESs give rise to vastly different drug delivery kinetics. The former necessitates fast delivery while the latter enables more sus-

tained release. Each platform allows for either low or high drug loading. Existing literature suggests that sustaining drug release is more important than increasing dose, at least for SIR DESs (Tzafriri et al., 2012). However, results from recent clinical trials of DCBs suggest that rapid drug release may, in certain circumstances, still be effective (Jeger et al., 2018). Moreover, existing literature highlights that the optimal drug release profile may be drug-dependent (Bozsak et al., 2014; Bozsak et al., 2015). Despite significant efforts over the past two decades, the optimal drug and release profile to successfully counteract restenosis remains ill-defined. Computational models, such as the one presented here, provide a platform for investigating spatio-temporal drug concentrations that are achieved in the arterial wall when different drugs and drug platforms with varying release kinetics are deployed. This, in turn, enables calculation and comparison of key indices related to safety (*DC*) and efficacy (%*SBSS*). In this paper, we have simulated drug delivery from DCBs and DESs, encompassing different drugs, doses and release kinetics. We now reiterate the key findings and their potential consequences.

Firstly, our results have highlighted that it is imperative to incorporate within the simulations the elevated pressure in the lumen during balloon application. This leads to deeper delivery of drug, higher drug retention and increased levels of specific binding site saturation, when compared with simulations that utilise a fixed lumen pressure for all time. Increasing the duration of DCB application from 30–60 s leads to higher *DC* and %*SBSS*. However, the relative increase in these values depends strongly on the DCB dose and release kinetics. In other words, the potential benefit of a DCB longer application time is dependent on the DCB configuration (drug, drug dose and excipient properties) and may therefore be more beneficial for some DCBs than for others. Our work has uncovered differences between SIR and PTX DCBs. Our results indicate that, assuming the same dose and release kinetics, SIR is retained within the tissue for longer than PTX, at least for the parameter values simulated.

The relatively rapid decline of *DC* values for the high dose SIR DCB, coupled with the high %*SBSS* levels suggests that the initial drug loading on the high dose SIR DCB may be too high: in other words, a lower initial drug dose could potentially give rise to similar levels of efficacy, while potentially easing any concerns regarding the high initial *DC* peak. On the other hand, the more prolonged decline of *DC* for the low dose SIR DCB, coupled with the less than ideal %*SBSS* levels suggests that the initial drug loading could be increased somewhat to achieve potentially greater efficacy, while potentially giving rise to *DC* peaks that are within safety margins. It is interesting to compare the peak *DC* achieved with these DCBs with existing in vivo experimental data. In (McKittrick et al., 2019), mean *DC* following SIR release from a low dose and high dose SIR DES was reported to range from approximately 5–10 μg/g tissue while in (Tzafriri et al., 2012), mean *DC* following SIR release from CYPHER and NEVO prototype DESs ranged from approximately 15–20 μg/g. However, as is common in the experimental literature, these peak measurements correspond to the first time point considered, 1 day, which is substantially later than the simulated peak for the low dose and high dose DCBs considered here. Grube and Buellesfield (Grube and Buellesfeld, 2006) do provide an earlier measurement time point of 1 h when considering release of a different compound, Biolimus A9™, from the BioMatrix™ stent platform. The mean *DC* peak at 1 h is reported to be approximately 600 μg/g, dropping to around 100 μg/g by 1 day. While each of these studies utilised porcine in vivo models, there are likely to be differences in the precise details of the experimental protocols. Availability of experimental data of *DC* following in vivo DCB deployment is more limited. Radke et al. (2011) consider a PTX DCB for coronary application and report a mean *DC* value of approximately 150 μg/g at 30 min post-deployment, which decreases to around 100 μg/g by 1 day and further reduces to around 100 μg/g by 7 days. Finally, Gongora et al. (Gongora et al., 2015) consider three PTX DCBs for peripheral applications (Ranger, In.Pact Admiral and Lutonix). They report mean *DC* peaks ranging from approximately 50–60 μg/g at 4 h, which drop to approximately 5–20 μg/g by 1 day and further drop to around 1–10 μg/g by 7 days. As well as possible differences in experimental protocols, the different anatomical location of the DCB deployment is likely to play a role. Thus, it appears that the *DC* values obtained in the present study are broadly in line with the existing literature, providing confidence in the simulations. Unfortunately, %*SBSS* is extremely difficult, if not impossible, to measure in vivo and we are not aware of any such measurements in the literature that would enable us to compare the values we have achieved in our simulations.

Returning to the direct comparison between DCBs and DESs, if saturating more specific binding sites earlier is most important, then each DCB considered offers an advantage over the realistic SIR DES simulated. However, if maintaining high levels of %*SBSS* towards and beyond 30 days is desired, then the realistic SIR DES would be preferred. By simulating an artificial fast SIR DES, we have demonstrated that if the safety and efficacy markers of the SIR DCBs simulated are acceptable, but a permanent structure is preferred, then it may be possible to design a new class of fast-release DES whose release kinetics are matched to those of a DCB.

Taken together, our findings suggest that there may exist a DCB configuration, in terms of drug loading and release rate, that gives rise to sufficiently similar safety and efficacy results as current commercial DESs such as the stent platform considered here. Future work should explore the use of an optimisation framework to attempt to infer DCB drug, dose and release rate, as well as procedural aspects such as balloon inflation pressure and application time, that give rise to *DC* values that fall within the therapeutic window, while maximising %*SBSS* for the period of arterial healing. Moreover, it may be worth investigating DCB and DES delivery within a single platform in an attempt to get the 'best of both worlds'.

Declaration of Competing Interest

We declare that one of our authors (Andre Fensterseifer Schmidt) has received a financial contribution towards his student fees from Biosensors International.

Acknowledgements

This work was funded by the Spanish Ministry of Economy, Industry and Competitiveness through research project number PID2019-107517RB-I00; the Department of Industry and Innovation (Government of Aragon) through research group Grant No. T24-20R (Fondo Social Europeo); and the Carlos III Health Institute (ISCIII) through the CIBER initiative. Dr. McGinty acknowledges funding provided by EPSRC (Grant No. EP/S030875/1 and EP/T017899/1).

Appendix A. Supplementary material

Supplementary data associated with this article can be found, in the online version, at https://doi.org/10.1016/j.ijpharm.2022.121742.

References

Ai, L., Vafai, K., 2006. A coupling model for macromolecule transport in a stenosed arterial wall. Int. J. Heat Mass Transf. 49 (9–10), 1568–1591.
Anbalakan, K., Toh, H.W., Ang, H.Y., Lindsay, B.M., Liang, L.H., 2021. Assessing the influence of atherosclerosis on drug coated balloon therapy using computational modelling. Eur. J. Pharmaceut. Biopharmaceut. 158, 72–82.
Bierer, B.E., Mattila, P.S., Standaert, R.F., Herzenberg, L.A., Burakoff, S.J., Crabtree, G., Schreiber, S.L., 1990. Two distinct signal transmission pathways in t lymphocytes are inhibited by complexes formed between an immunophilin and either fk506 or rapamycin. Proc. Natl. Acad. Sci. 87 (23), 9231–9235.
Bozsak, F., Chomaz, J.-M., Barakat, A.I., 2014. Modeling the transport of drugs eluted from stents: physical phenomena driving drug distribution in the arterial wall. Biomech. Model. Mechanobiol. 13 (2), 327–347.
Bozsak, F., Gonzalez-Rodriguez, D., Sternberger, Z., Belitz, P., Bewley, T., Chomaz, J.-M., Barakat, A.I., 2015. Optimization of drug delivery by drug-eluting stents. PLoS One 10 (6), e0130182.

Byrne, R.A., Joner, M., Kastrati, A., 2015. Stent thrombosis and restenosis: what have we learned and where are we going? the andreas grüntzig lecture esc 2014. Eur. Heart J. 36 (47), 3320–3331.
Byrne, R.A., Serruys, P.W., Baumbach, A., Escaned, J., Fajadet, J., James, S., Joner, M., Oktay, S., Jüni, P., Kastrati, A., et al., 2015. Report of a european society of cardiology-european association of percutaneous cardiovascular interventions task force on the evaluation of coronary stents in europe: executive summary. Eur. Heart J. 36 (38), 2608–2620.
Chang, G.H., Azar, D.A., Lyle, C., Chitalia, V.C., Shazly, T., Kolachalama, V.B., 2019. Intrinsic coating morphology modulates acute drug transfer in drug-coated balloon therapy. Scient. Rep. 9 (1), 1–10.
Colombo, M., Corti, A., Berceli, S., Migliavacca, F., McGinty, S., Chiastra, C., 2021. 3d modelling of drug-coated balloons for the treatment of calcified superficial femoral arteries. Plos One 16 (10), e0256783.
Cortese, B., Bertoletti, A., 2011. Paclitaxel coated balloons for coronary artery interventions: A comprehensive review of preclinical and clinical data. Int. J. Cardiol. 161, 4–12.
Creel, C.J., Lovich, M.A., Edelman, E.R., 2000. Arterial paclitaxel distribution and deposition. Circ. Res. 86 (8), 879–884.
Díaz, J.F., Barasoain, I., Andreu, J.M., 2003. Fast kinetics of taxol binding to microtubules effects of solution variables and microtubule-associated proteins. J. Biol. Chem. 278 (10), 8407–8419.
Escuer, J., Cebollero, M., Pena, E., McGinty, S., Martínez, M.A., 2020. How does stent expansion alter drug transport properties of the arterial wall? J. Mech. Behav. Biomed. Mater., 103610
Escuer, J., Aznar, I., McCormick, C., Peña, E., McGinty, S., Martinez, M.A., 2021. Influence of vessel curvature and plaque composition on drug transport in the arterial wall following drug-eluting stent implantation. Biomech. Model. Mechanobiol. 20 (2), 767–786.
Formaggia, L., Quarteroni, A., Veneziani, A., 2010. Cardiovascular Mathematics: Modeling and simulation of the circulatory system, volume 1. Springer Science & Business Media.
Gongora, C.A., Shibuya, M., Wessler, J.D., McGregor, J., Tellez, A., Cheng, Y., Conditt, G. B., Kaluza, G.L., Granada, J.F., 2015. Impact of paclitaxel dose on tissue pharmacokinetics and vascular healing: a comparative drug-coated balloon study in the familial hypercholesterolemic swine model of superficial femoral in-stent restenosis. JACC: Cardiovasc. Intervent. 8 (8), 1115–1123.
Grube, E., Buellesfeld, L., 2006. Biomatrix biolimus a9-eluting coronary stent: a next-generation drug-eluting stent for coronary artery disease. Exp. Rev. Med. Dev. 3 (6), 731–741.
Heilmann, T., Richter, C., Noack, H., Post, S., Mahnkopf, D., Figulla, H., 2010. Drug release profiles of different drug-coated balloon platforms. Eur. Cardiol. 6 (4), 40–44.
Hwang, C.-W., Edelman, E.R., 2002. Arterial ultrastructure influences transport of locally delivered drugs. Circ. Res. 90 (7), 826–832.
Hwang, C.-W., David, Wu., Edelman, E.R., 2001. Physiological transport forces govern drug distribution for stent-based delivery. Circulation 104 (5), 600–605.
Hwang, C.-W., David, Wu., Edelman, E.R., 2003. Impact of transport and drug properties on the local pharmacology of drug-eluting stents. Int. J. Cardiovasc. Intervent. 5 (1), 7–12.
Jain, A., McGinty, S., Pontrelli, G., Zhou, L., 2022. Theoretical modeling of endovascular drug delivery into a multilayer arterial wall from a drug-coated balloon. Int. J. Heat Mass Transf. 187, 122572.
Jeger, R.V., Farah, A., Ohlow, M.-A., Mangner, N., Möbius-Winkler, S., Leibundgut, G., Weilenmann, D., Wöhrle, J., Richter, S., Schreiber, M., et al., 2018. Drug-coated balloons for small coronary artery disease (basket-small 2): an open-label randomised non-inferiority trial. The Lancet 392 (10150), 849–8568.
Karner, G., Perktold, K., Zehentner, H.P., 2001. Computational modeling of macromolecule transport in the arterial wall. Comput. Methods Biomech. Biomed. Eng. 4 (6), 491–504.
Kedem, O., Katchalsky, A., 1958. Thermodynamic analysis of the permeability of biological membranes to non-electrolytes. Biochim. Biophys. Acta 27, 229–246.
Kolachalama, V.B., Pacetti, S.D., Franses, J.W., Stankus, J.J., Zhao, H.Q., Shazly, T., Nikanorov, A., Schwartz, L.B., Tzafriri, A.R., Edelman, E.R., 2013. Mechanisms of tissue uptake and retention in zotarolimus-coated balloon therapy. Circulation 127 (20), 2047–2055.
Lee, D.-H., de la Torre Hernandez, J.M., 2018. The newest generation of drug-eluting stents and beyond. Eur. Cardiol. Rev. 13 (1), 54.
Levin, A.D., Vukmirovic, N., Hwang, C.-W., Edelman, E.R., 2004. Specific binding to intracellular proteins determines arterial transport properties for rapamycin and paclitaxel. Proc. Natl. Acad. Sci. USA 101 (25), 9463–9467.
Levitt, D.G., 1975. General continuum analysis of transport through pores. i. proof of onsager's reciprocity postulate for uniform pore. Biophys. J . 15 (6), 533–551.
Lovich, M.A., Edelman, E.R., 1996. Computational simulations of local vascular heparin deposition and distribution. Am. J. Physiol.-Heart Circul. Physiol. 271 (5), H2014–H2024.
Mandal, P.K., Sarifuddin, Kolachalama, V.B., 2016. Computational model of drug-coated balloon delivery in a patient-specific arterial vessel with heterogeneous tissue composition. Cardiovasc. Eng. Technol. 7 (4), 406–419.
McGinty, S., 2014. A decade of modelling drug release from arterial stents. Math. Biosci. 257, 80–90.
McGinty, S., Pontrelli, G., 2016. On the role of specific drug binding in modelling arterial eluting stents. J. Math. Chem. 54 (4), 967–976.
McKittrick, C.M., McKee, S., Kennedy, S., Oldroyd, K., Wheel, M., Pontrelli, G., Dixon, S., McGinty, S., McCormick, C., 2019. Combining mathematical modelling with in vitro experiments to predict in vivo drug-eluting stent performance. J. Controlled Release 303, 151–161.
McQueen, A., Escuer, J., Aggarwal, A., Kennedy, S., McCormick, C., Oldroyd, K., McGinty, S., 2021. Do we really understand how drug eluted from stents modulates arterial healing? Int. J. Pharm. 601, 120575.
Meyer, G., Merval, R., Tedgui, A., 1996. Effects of pressure-induced stretch and convection on low-density lipoprotein and albumin uptake in the rabbit aortic wall. Circ. Res. 79 (3), 532–540.
Mongrain, R., Leask, R., Brunette, J., Faik, I., Bulman-Feleming, N., Nguyen, T., 2005. Numerical modeling of coronary drug eluting stents. Stud. Health Technol. Inform. 113, 443–458.
Perkins, L.E.L., Boeke-Purkis, K.H., Wang, Q., Stringer, S.K., Coleman, L.A., 2009. Xience v™ everolimus-eluting coronary stent system: A preclinical assessment. J. Intervent. Cardiol. 22, S28–S40.
Radke, P.W., Joner, M., Joost, A., Byrne, R.A., Hartwig, S., Bayer, G., Steigerwald, K., Wittchow, E., 2011. Vascular effects of paclitaxel following drug-eluting balloon angioplasty in a porcine coronary model: the importance of excipients. EuroIntervention 7 (6), 730–737.
Rami Tzafriri, A., Levin, A.D., Edelman, E.R., 2009. Diffusion-limited binding explains binary dose response for local arterial and tumour drug delivery. Cell Prolif. 42 (3), 348–363.
Roth, G.A., Abate, D., Abate, K.H., Abay, S.M., Abbafati, C., Abbasi, N., Abbastabar, H., Abd-Allah, F., Abdela, J., Abdelalim, A., et al., 2018. Global, regional, and national age-sex-specific mortality for 282 causes of death in 195 countries and territories, 1980–2017: a systematic analysis for the global burden of disease study 2017. The Lancet 392 (10159), 1736–1788.
Sarifuddin, Mandal, P.K., 2018. Effect of interstitial fluid flow on drug-coated balloon delivery in a patient-specific arterial vessel with heterogeneous tissue composition: A simulation study. Cardiovasc. Eng. Technol. 9 (2), 251–267.
Scheller, B., Hehrlein, C., Bocksch, W., Rutsch, W., Haghi, D., Dietz, U., Böhm, M., Speck, U., 2006. Treatment of coronary in-stent restenosis with a paclitaxel-coated balloon catheter. N. Engl. J. Med. 355 (20), 2113–2124.
Sojitra, P., Yazdani, S., Otsuka, F., Doshi, M., Kolodgie, F., Virmani, R., 2013. Crt-123. a novel nano particle sirolimus delivery via coated balloon. JACC: Cardiovasc. Intervent. 6 (2 Suppl S), S40.
Tzafriri, A.R, Adam Groothuis, G., Price, S., Edelman, E.R., 2012. Stent elution rate determines drug deposition and receptor-mediated effects. J. Controlled Release 161 (3), 918–926.
Tzafriri, A.R., Parikh, S.A., Edelman, E.R., 2019. Taking paclitaxel coated balloons to a higher level: Predicting coating dissolution kinetics, tissue retention and dosing dynamics. J. Controlled Release 310, 94–102.
Tzafriri, A.R., Muraj, B., Garcia-Polite, F., Salazar-Martín, A.G., Markham, P., Zani, B., Spognardi, A., Albaghdadi, M., Alston, S., Edelman, E.R., 2020. Balloon-based drug coating delivery to the artery wall is dictated by coating micro-morphology and angioplasty pressure gradients. Biomaterials 260, 120337.
Vairo, G., Cioffi, M., Cottone, R., Dubini, G., Migliavacca, F., 2010. Drug release from coronary eluting stents: a multidomain approach. J. Biomech. 43 (8), 1580–1589.
Wear, M.A., Walkinshaw, M.D., 2007. Determination of the rate constants for the fk506 binding protein/rapamycin interaction using surface plasmon resonance: An alternative sensor surface for ni2+–nitrilotriacetic acid immobilization of his-tagged proteins. Anal. Biochem. 371 (2), 250–252.
Zunino, P., 2004. Multidimensional pharmacokinetic models applied to the design of drug-eluting stents. Cardiovasc. Eng.: An Int. J. 4 (2), 181–191.